CORA Cork Open Research Archive
Cartlann Taighde Oscailte Chorcaí

Title	Contactless electroreflectance study of the surface potential barrier in n-type and p-type InAlAs van Hoof structures lattice matched to InP
Authors	Tolloczko, Agata;Kopaczek, Jan;Szukiewicz, Rafal;Gocalińska, Agnieszka M.;Pelucchi, Emanuele;Hommel, Detlef;Kudrawiec, Robert
Publication date	2018-04-19
Original Citation	Tolloczko, A., Kopaczek, J., Szukiewicz, R., Gocalinska, A., Pelucchi, E., Hommel, D. and Kudrawiec, R.(2018) 'Contactless electroreflectance study of the surface potential barrier in n-type and p-type InAlAs van Hoof structures lattice matched to InP', Journal of Physics D: Applied Physics, 51(21), p.215104 (24pp). https://doi.org/10.1088/1361-6463/aabf6b
Type of publication	Article (peer-reviewed)
Link to publisher's version	http://iopscience.iop.org/article/10.1088/1361-6463/aabf6b - 10.1088/1361-6463/aabf6b
Rights	© 2018 IOP Publishing Ltd. This is an author-created, un-copyedited version of an article accepted for publication in Journal of Physics D: Applied Physics. The publisher is not responsible for any errors or omissions in this version of the manuscript or any version derived from it. The Version of Record is available online at https://doi.org/10.1088/1361-6463/aabf6b. - http://creativecommons.org/licenses/by-nc-nd/3.0/
Download date	2026-11-04 10:03:56
Item downloaded from	https://hdl.handle.net/10468/5873



University College Cork, Ireland
Coláiste na hOllscoile Corcaigh

Journal of Physics D: Applied Physics

ACCEPTED MANUSCRIPT

Contactless electroreflectance study of the surface potential barrier in n-type and p-type InAlAs van Hoof structures lattice matched to InP

To cite this article before publication: Agata Tolloczko *et al* 2018 *J. Phys. D: Appl. Phys.* in press https://doi.org/10.1088/1361-6463/aabf6b

Manuscript version: Accepted Manuscript

Accepted Manuscript is "the version of the article accepted for publication including all changes made as a result of the peer review process, and which may also include the addition to the article by IOP Publishing of a header, an article ID, a cover sheet and/or an 'Accepted Manuscript' watermark, but excluding any other editing, typesetting or other changes made by IOP Publishing and/or its licensors"

This Accepted Manuscript is **© 2018 IOP Publishing Ltd**.

During the embargo period (the 12 month period from the publication of the Version of Record of this article), the Accepted Manuscript is fully protected by copyright and cannot be reused or reposted elsewhere.
As the Version of Record of this article is going to be / has been published on a subscription basis, this Accepted Manuscript is available for reuse under a CC BY-NC-ND 3.0 licence after the 12 month embargo period.

After the embargo period, everyone is permitted to use copy and redistribute this article for non-commercial purposes only, provided that they adhere to all the terms of the licence https://creativecommons.org/licences/by-nc-nd/3.0

Although reasonable endeavours have been taken to obtain all necessary permissions from third parties to include their copyrighted content within this article, their full citation and copyright line may not be present in this Accepted Manuscript version. Before using any content from this article, please refer to the Version of Record on IOPscience once published for full citation and copyright details, as permissions will likely be required. All third party content is fully copyright protected, unless specifically stated otherwise in the figure caption in the Version of Record.

View the article online for updates and enhancements.

This content was downloaded from IP address 143.239.102.113 on 25/04/2018 at 09:49

Contactless electroreflectance study of the surface potential barrier in *n*-type and *p*-type InAlAs van Hoof structures lattice matched to InP

A. Tolloczko[1], J. Kopaczek[1], R. Szukiewicz[2], A. Gocalińska[3], E. Pelucchi[3], D. Hommel[2], and R. Kudrawiec[1, 2 a)]

[1]*Faculty of Fundamental Problems of Technology, Wroclaw University of Science and Technology, Wybrzeże Wyspiańskiego 27, 50-370 Wrocław, Poland*

[2]*Wroclaw Research Center EIT+ Sp. z o.o., ul. Stabłowicka 147, 54-066 Wrocław, Poland*

[3]*Tyndall National Institute, University College Cork, „Lee Maltings", Dyke Parade, Cork, Ireland*

N-type and *p*-type $In_{0.52}Al_{0.48}As$ van Hoof structures with various thicknesses of undoped $In_{0.52}Al_{0.48}As$ layer (30, 60, 90, and 120 nm) were grown by metal-organic vapor phase epitaxy on InP substrates and studied by contactless electroreflectance (CER) at room temperature. The InAlAs bandgap related CER resonance followed by a strong Franz-Keldysh oscillation (FKO) of various periods was observed clearly for the two structures. This period was decreased with the decrease of thickness of undoped $In_{0.52}Al_{0.48}As$ layer and was slightly narrower for *p*-type structures. The FKO period analysis indicates that the Fermi level is pinned 0.73±0.02 eV below the conduction band at $In_{0.52}Al_{0.48}As$ surface. This pinning was attributed to the surface reconstruction combined with the adsorption of oxygen and carbon atoms (consequence of air exposure) which were detected on the $In_{0.52}Al_{0.48}As$ surface by X-ray photoelectron spectroscopy. Also, CER measurements repeated one year after the sample growth shows that the process of InAlAs oxidation in laboratory ambient is negligible and therefore this alloy can be used as a protective cap layer in InP-based heterostructures.

a) E-mail address: robert.kudrawiec@pwr.edu.pl

Accepted Manuscript

I. INTRODUCION

$In_{1-x}Al_xAs$ with x = 48% (InAlAs from now on) can be grown lattice-matched to InP, making it a relevant component for many important applications such as telecom lasers [1], InP-based high electron mobility transistors or/and other high frequency devices [2, 3]. This alloy is also the natural candidate for claddings, barriers, and waveguides in InP-based quantum cascade lasers [4, 5], and recently InAlAs was used as an absorber in InP-based multijunction solar cells [6, 7]. In addition InAlAs could be used as a capping layer for protecting InP-based heterostructures from oxidation instead of exploiting other layers such as InGaAs lattice matched to InP (which has a very narrow bandgap) or InP itself, which, for example, is impossible to grow in an MBE systems without specialized P sources. However InAlAs is not routinely used for this purpose, as a strong oxidation is generally expected due to the presence of Al in this alloy, in analogy to AlGaAs which does oxidize heavily when air exposed.

Indeed, the issue of InAlAs oxidation has never been extensively explored so far and therefore little is known about its long term stability when air exposed. Moreover the surface potential barrier for this alloy (i.e., the Fermi level position at the InAlAs surface) is also unknown and so its modification with time upon oxidation.

The aim of this paper is to clarify these issues, by analyzing InAlAs (as discussed lattice matched to InP) surface potential barrier by contactless electroreflectance (CER).

Among several methods allowing determining the surface potential barrier, CER is considered highly suitable [8, 9]. In contrast to techniques involving measurements of I-V or C-V characteristics of the metal/semiconductor interface [10, 11], CER does not require metal contacts on the semiconductor surface and thus does not affect its morphology and thereby can probe the surface potential barrier for the as-grown material without any surface treatment, as well as the surface potential barrier after air exposure. So far only photoreflectance spectroscopy, which has similarities to CER spectroscopy, has been applied to study heavily doped $In_{0.52}Al_{0.48}As$ samples grown by molecular beam epitaxy on InP (Fe) substrates, but the surface potential barrier was not determined for those samples [12], and in general the study of the Fermi-level position on the surface has not

Accepted Manuscript

yet been extended to InAlAs. In order to perform a careful study of surface potential barrier for InAlAs lattice matched to InP and its change with time due to possible surface degradation, two sets of *n*-type and *p*-type InAlAs van Hoof structures [13] lattice matched to InP were grown and studied by CER spectroscopy, which together with a number of other characterization techniques allowed us to determine both a good estimation of the Fermi level pinning position, its stability with air exposure in time, hence its (unexpected) suitability as capping layer.

II. EXPERIMENT

The InAlAs samples were grown by metal-organic vapor phase epitaxy (MOVPE) at low pressure (80 mbar) in a commercial horizontal reactor with purified N_2 as carrier gas and trimethylindium (TMIn), trimethylaluminium (TMAl), arsine (AsH_3) and phosphine (PH_3) as precursors. [14, 15]. The structures were grown on semi-insulating (Fe-doped) (100)+/- 0.02° epiready InP substrates and contain 100 nm nominally undoped InP buffer, followed by 200 nm thick *n*-type (or *p*-type) InAlAs layer, and undoped top InAlAs layer of different thickness (30, 60, 90, or 120 nm). These InAlAs layers are lattice matched to InP. S_4H_6 and CBr_4 were used for *n*-type and *p*-type doping, respectively. Majority carrier concentration is similar in both types of samples: 4.1 x 10^{18} cm^{-3} for *n*-type and 3.5 x 10^{18} cm^{-3} for *p*-type. In the undoped InAlAs layers the residual carrier concentration is below 10^{17} cm^{-3}. The sketch of layers in the InAlAs van Hoof structures (i.e., structures with undoped cap layer where a homogeneous built-in electric field is expected) is depicted in Fig. 1 (a) and the expected band bending in *n*-type and *p*-type structures in panel (b) and (c), respectively.

For CER measurements the samples were placed in a capacitor with a half-transparent wire mesh top electrode [16]. The top electrode was set at a distance of ~0.5 mm from the sample surface to both avoid short circuit and provide strong enough electric field. A ~3.0 kV alternating voltage was applied to the electrodes at a frequency of 290 Hz. All measurements were performed in ambient air at room temperature. Other relevant details of the CER set-up can be found in Ref. [16].

Accepted Manuscript

For piezoreflectance (PzR) measurements samples were glued on piezo-ceramics by acrylic glue. An AC voltage with amplitude 300 V and frequency 280 Hz was applied to the piezo-ceramics in order to modulate sample strain.

For accurate identification of surface composition X-ray photoelectron spectroscopy (XPS) was utilized: samples were placed on a double glue copper foil and mounted on a sample holder. After that they were introduced to a load lock and at ~10^{-8} mbar level (~ one hour) they were introduced into the analysis chamber. XPS spectra were acquired using a SCIENTA hemispherical photoelectron spectrometer equipped with a monochromatic AlKα source operating at 300 W. The base pressure in the analysis chamber was better than $1x10^{-10}$ mbar. Charge compensation was achieved using a flood source. All acquired high resolution spectra were calibrated to adventitious carbon at 285 eV. High resolution spectra were measured with a pass energy of 200 eV. The overall resolution of the spectrometer in this operating mode was 0.70 eV as measured by the full width of half maximum (FWHM) of the $Ag3d_{5/2}$ line. After subtraction of the Shirley-type background, the core-level spectra were decomposed into their components with mixed Gaussian–Lorentzian lines (70% G + 30% L for majority of photo-peaks) following a non-linear least squares curve-fitting procedure, using the CasaXPS software. BE and FWHM of the components and their areas were determined from the fitting results.

III. RESUTS AND DISCUSSION

Figure 2 and 3 show CER spectra of *n*-type and *p*-type InAlAs van Hoof structures, respectively, measured at room temperature. Color lines correspond to measurements a few days after the sample growth while the grey lines correspond to measurements performed about one year later at similar conditions. For *p*-type samples a band gap related transition in the InP buffer layer is visible at ~1.35 eV. Such transition is not observed for *n*-type samples, because of a lack of band bending modulation in the InP buffer in these samples. It is associated with a better screening of InP buffer by *n*-type layer from the external modulation. For all samples a strong CER resonance related

Accepted Manuscript

to band-to-band absorption in the undoped InAlAs layer is observed at ~1.45 eV. This resonance is followed by Franz-Kieldysh oscillations (FKOs) associated to the built-in electric field in the undoped InAlAs layer. Indeed, as it is well known, a homogeneous built-in electric field exists in the undoped InAlAs layer due to the Fermi level positioning close to the conduction (valence) band in the *n*-type (*p*-type) doped InAlAs layer and the specific Fermi level pinning at the InAlAs surface. This determines the surface potential barrier. Since the thickness of undoped InAlAs layer is changing in the studied samples, so does the built-in electric field and hence the period of the FKOs varies as reported in Figs. 2 and 3.

The value of the built-in electric field can be extracted from the period of the FKOs. The relation between the build-in electric field and the FKO period is described using an asymptotic expression for electro-reflectance [17]

$$\frac{\Delta R}{R} \propto \exp\left[\frac{-2\Gamma\sqrt{E-E_g}}{(\hbar\theta)^{3/2}}\right] \cdot cos\left[\frac{4}{3}\left(\frac{E-E_g}{\hbar\theta}\right)^{3/2} + \varphi\right] \cdot \frac{1}{E^2(E-E_g)}$$

$$(\hbar\theta)^3 = \frac{e^2\hbar^2F^2}{2\mu} \quad (1)$$

where $\hbar\theta$ is the electro-optic energy, Γ is the linewidth, φ is an angle, F is the electric field and μ is the electron-hole reduced mass, assumed to be 0.083 m_0 [18]. The FKOs extrema are given by

$$n\pi = \varphi + \frac{4}{3}\left(\frac{E_n-E_g}{\hbar\theta}\right)^{3/2} \quad (2)$$

where n is an index of n-th extremum and E_n is corresponding energy.

In order to precisely determine and verify the bandgap of the InAlAs layers, which is required for the FKO period analysis, PzR spectra have been measured for the studied samples. An example of PzR spectrum is shown in the inset in Fig. 2. In this case a single resonance related to the bandgap absorption in InP and InAlAs is clearly visible. PzR spectra are not affected by FKOs because of other mechanism of reflectance modulation (i.e., modulation of the lattice constant instead of the built-in electric field) and thereby have been elected for determining the bandgap. Here, PzR spectra have been fitted by the Aspnes formula [19] which is widely used to analyze modulated reflectance spectra [20-22]. The resulting bandgap is 1.435 eV and corresponds to literature data reviewed in

Accepted Manuscript

Ref. [18], but it should be noted that this value is 25 meV lower than the bandgap calculating from the parameters recommended in Ref. [18].

Figure 4 (a) and (b) shows a detailed analysis of the InAlAs-related FKO period and associated built-in electric field for both the *n*-type and *p*-type InAlAs van Hoof structures, respectively. We determined that the built-in electric field equals ~ 217, 113, 82, and 58 kV/cm for *n*-type structures with 30, 60, 90, and 120 nm thick undoped layer, respectively. Slightly weaker built-in electric fields have been found for the *p*-type structures: ~181, 92, 68, and 43 kV/cm for samples with 30, 60, 90, and 120 nm thick undoped layer, respectively.

We also observe that since the shape of a CER resonance is sensitive to the type of band bending [9, 23], the opposite phase observed for the two sets of heterostructures (see green arrows in Figs. 2 and 3) means an opposite sign of the built-in electric field, as expected and as also schematically shown in Fig. 1.

At first approximation the built-in electric field in van Hoof structures is given by the following formula: $F = \frac{E_\phi}{d}$ for *n*-type and $F = \frac{E_g - E_\phi}{d}$ for *p*-type structures, where d is the thickness of the undoped InAlAs layer, F is the built-in electric field extracted from the FKO analysis, and E_ϕ is the Fermi level position at the InAlAs surface defined as in Fig.1. The obtained built-in electric fields have been plotted in Fig. 5 and fitted by the above formula with E_ϕ treated as a free parameter. E_ϕ has been estimated to be ~0.64 eV and ~0.88 eV for *n*-type and *p*-type structures, respectively.

The derived Fermi-level position on InAlAs surface can be underestimated because of some depletion of the doped InAlAs layer at the InAlAs(cap)/InAlAs:Si(C) interface. Indeed, the presence of a depletion region causes leaking of a non-uniform electric field into the doped layer, which can be considered, simplifying, as an increase of the effective thickness of the layer in which the built-in electric field is present. In order to include these adjustments, calculations of the band bending in both structures have been performed using Nextnano software [24]. Treating the Fermi-level position on InAlAs surface as a free parameter, the distribution of built-in electric field in the undoped InAlAl layer was analyzed. The results for *n*-type and *p*-type structures are shown in Fig.

Accepted Manuscript

6 (a) and (b), respectively, where thin solid lines show theoretical dependency of electric field versus the Fermi-level position on InAlAs surface and thick solid horizontal lines correspond to experimental values of electric field determined by CER measurements. The best compliance with the experiment is obtained assuming $E_\phi = 0.73 \pm 0.02\ eV$ for both types of van Hoof structures, which indicates that Fermi-level pinning at InAlAs surface is close to the middle of energy gap, but slightly closer to the conduction band.

Figures 7 shows the band bending in the examined structures, calculated for the value of $E_\phi = 0.73eV$. It can be noticed that the depletion region (marked as a gray field) is the most significant for structures with thin cap layer. As d increases, the depletion layer is getting thinner and its contribution to the sample area with the built-in electric field is less important. Moreover it is visible that the built-in electric field is homogeneous in the undoped InAlAs layer and the simple estimation of Fermi level position from the $E_\phi = Fd$ formula is acceptable at the first approximation.

The derived Fermi-level position at InAlAs surface at very similar energies for *n*-type and *p*-type structures means that, as largely expected, the Fermi level is indeed pinned at a singularity of density of states partially occupied by electrons. Such a density of states is generally linked to surface reconstruction and adsorption of foreign atoms. In order to gain further insights, XPS measurements were performed.

Figure 8 shows an atomic concentration of a surface atoms identified on two *n*-type and *p*-type InAlAs van Hoof structures. As an example the XPS spectrum recorded for one of the *n*-type van Hoof structures is shown in the inset of Fig. 8. This shows, besides the expected Al, In, and As atoms, not surprising, significant concentration of oxygen and carbon exist on the surface of the investigated samples, as it broadly found with other III-V semiconductors, which generally points at a possible role in the pinning of Fermi level. More interesting, samples measured one year after the growth, and stored in ambient atmosphere, present CER spectra very similar to those measured a few days after growth (compare color and grey lines in Figs. 2 and 3), indicating stable Fermi level pinning and its early stage establishment.

Accepted Manuscript

It is worth noting that this is not always the case. CER spectra for AlGaAs structures change very significantly with time due to oxidation of AlGaAs layer. In the investigated InAlAs van Hoof structures a heavy oxidation of undoped InAlAs layer should be accompanied with an increase of built-in electric field (an increase of the FKO period) due to a reduction of the thickness of the undoped InAlAs layer. Such an effect should be observed in case of further oxidation of InAlAs layer with the time after the growth, but is not observed for the investigated samples, indicating that the process of InAlAs oxidation in laboratory ambient is negligible. This is in line with previous observations that the oxidation process of many epitaxial III-V materials (with the well-known exception of AlGaAs or AlAs) affects only several initial monolayers, with a time-dependent oxide type change, but with not necessarily significant thickness' increase. [25]. Also detailed AFM investigation of multiple InAlAs samples from laboratory history, kept on showing distinct crystallographic steps, even on significantly aged samples (see Fig. 9), i.e. the oxidation process did not significantly perturb the overall surface morphology. Therefore the alloy can be successfully used as a cap protective layer in InP-based heterostructures.

IV. CONCLUSIONS

In summary, *n*-type and *p*-type $In_{0.52}Al_{0.48}As$ van Hoof structures were grown by MOVPE in order to study the Fermi level position at $In_{0.52}Al_{0.48}As$ surface by CER spectroscopy. It has been found that the Fermi level is pinned 0.73 ± 0.02 eV below the conduction band for both *n*-type and *p*-type structures. CER measurements repeated one year after the sample growth shows that the Fermi-level is still located at the same energy. It suggests that the process of InAlAs oxidation in laboratory ambient is negligible in contrast, for example, to the oxidation of AlGaAs alloy of similar aluminum content. Therefore InAlAs lattice matched to InP can be used as a protective cap layer in InP-based heterostructures.

ACKNOWLEDGMENTS

Accepted Manuscript

J. K. acknowledges for support within the IUVENTUS PLUS grant no. IP2015 034774 from the Ministry of Science and Higher Education in Poland; E.P. and A.G. acknowledge support by Science Foundation Ireland under grants 12/RC/2276, 10/IN.1/I3000 and 15/IA/2864.

Accepted Manuscript

References

[1] Ch. L.M. Daunt, H. Yang, W. Han, K. Thomas, E. Pelucchi, B. Corbett, and F. H. Peters, Dielectric free fabrication of compact 30 GHz photodetectors using the isolated pedestal contact configuration, IEEE Photon. Technol. Lett. **24**, 1082 (2012)

[2] D. Moro-Melgar, J. Mateos, T. González, and B. G. Vasallo, Effect of tunnel injection through the Schottky gate on the static and noise behavior of GaInAs/AlInAs high electron mobility transistor, J. Appl. Phys. **116**, 234502 (2014).

[3] J. Ajayan and D. Nirmal A review of InP/InAlAs/InGaAs based transistors for high frequency applications, Superlattices and Microstructures **86**, 1–19 (2015).

[4] Ch. A. Wang, B. Schwarz, D. F. Siriani, L. J. Missaggia, M. K. Connors, T. S. Mansuripur, D. R. Calawa, D. McNulty, M. Nickerson, J. P. Donnelly, K. Creedon, and F. Capasso, MOVPE Growth of LWIR AlInAs/GaInAs/InP Quantum Cascade Lasers: Impact of Growth and Material Quality on Laser Performance, IEEE J. Select. Topics Quant. Electron. **23**, 1200413 (2017).

[5] P. Gutowski, I. Sankowska, P. Karbownik, D. Pierscinska, O. Serebrennikova, M. Morawiec, E. Pruszynska-Karbownik, K. Gołaszewska-Malec, K. Pierscinski, J. Muszalski, and M. Bugajski, MBE growth of strain-compensated InGaAs/InAlAs/InP quantum cascade, J. Cryst. Growth **466**, 22–29 (2017)

[6] M. S. Leite, R. L. Woo, J. N. Munday, W. D. Hong, S. Mesropian, D. C. Law, and H. A. Atwater, Towards an optimized all lattice-matched InAlAs/InGaAsP/InGaAs multijunction solar cell with efficiency >50%, Appl. Phys. Lett. **102**, 033901 (2013).

[7] B. L. Smith, Z. S. Bittner, S. D. Hellstroem, G. T. Nelson, M. A. Slocum, A. G. Norman, D. V. Forbes, and S. M. Hubbard, InAlAs photovoltaic cell design for high device efficiency, Prog. Photovolt: Res. Appl. **25**, 706–713 (2017).

Accepted Manuscript

[8] R. Kudrawiec, H.P. Nair, M. Latkowska, J. Misiewicz, S.R. Bank, and W. Walukiewicz, Contactless electroreflectance study of the Fermi level pinning on GaSb surface in n-type and p-type GaSb Van Hoof structures, J. Appl. Phys. **112**, (2012).

[9] Ł. Janicki, M. Gładysiewicz, J. Misiewicz, K. Klosek, M. Sobanska, P. Kempisty, Z.R. Zytkiewicz, and R. Kudrawiec, Contactless electroreflectance studies of the Fermi level position at the air/GaN interface: Bistable nature of the Ga-polar surface, Appl. Surf. Sci. **396**, 1657 (2017).

[10] F. Gueissaz, M. Gailhanou, R. Houdré, and M. Ilegems, Measurements of Al-AlInAs Schottky barriers prepared in situ by molecular beam epitaxy, Appl. Phys. Lett. **60**, 1099 (1992).

[11] S. Fujita, S. Naritsuka, T. Noda, A. Wagai, and Y. Ashizawa, Barrier height lowering of Schottky contacts on AlInAs layers grown by metal-organic chemical-vapor deposition, J. Appl. Phys. **73**, 1284 (1993).

[12] E. Laureto, I.F.L. Dias, J.L. Duarte, M. Di, H. Iwamoto, M.T.P. Freitas, S.A. Lourenço, F. Toginho, and J.C. Harmand, Investigation of optical properties of interfaces between heavily doped $Al_{0.48}In_{0.52}As$:Si and InP (Fe) substrates by photoreflectance analysis, J. Appl. Phys. **85**, 4184 (1999).

[13] C. Van Hoof, K. Deneffe, J. De Boeck, D. J. Arent, and G. Borghs, Franz–Keldysh oscillations originating from a well-controlled electric field in the GaAs depletion region, Appl. Phys. Lett. **54**, 608 (1989)

[14] V. Dimastrodonato, L. O. Mereni, R. J. Young, and E. Pelucchi, Relevance of the purity level in a Metal Organic Vapour Phase Epitaxy reactor environment for the growth of high quality pyramidal site-controlled Quantum Dots, J. Cryst. Growth **315**, 119 (2011).

[15] A. Gocalinska, M. Manganaro, E. Pelucchi and D.D. Vvedensky, Surface organization of homoepitaxial InP films grown by metalorganic vapor-phase epitaxy, Phys. Rev. B 86, 165307 (2012).

Accepted Manuscript

[16] R. Kudrawiec, Application of contactless electroreflectance to III-nitrides, Phys. Status Solidi (b) **247**, 1616 (2010).

[17] D. E. Aspnes and A. A. Studna, Schottky-Barrier Electroreflectance: Application to GaAs. Phys. Rev. B **7**, 4605–4625 (1973).

[18] I. Vurgaftman, J. R. Meyer, and L. R. Ram-Mohan, Band parameters for III–V compound semiconductors and their alloys, J. Appl. Phys. **89**, 5815 (2001).

[19] D. E. Aspnes, Third-derivative modulation spectroscopy with low-field electroreflectance, Surf. Sci. **37**, 418 (1973).

[20] J. Misiewicz and R. Kudrawiec, Contactless electroreflectance spectroscopy of optical transitions in low dimensional semiconductor structures, Opto-Electronics Review **20**, 101 (2012).

[21] K. Żelazna, M. P. Polak, P. Scharoch, J. Serafinczuk, M. Gladysiewicz, J. Misiewicz, J. Dekoster, R. Kudrawiec, Electronic band structure of compressively strained $Ge_{1-x}Sn_x$ with x<0.11 studied by contactless electroreflectance, Appl. Phys. Lett. **106**, 142102 (2015).

[22] F. Dybała, M. P. Polak, J. Kopaczek, P. Scharoch K. Wu, S. Tongay, R. Kudrawiec, Pressure coefficients for direct optical transitions in MoS_2, $MoSe_2$, WS_2, and WSe_2 crystals and semiconductor to metal transitions, Scientific Reports **6**, 26663 (2016).

[23] R. Kudrawiec, M. Motyka, J. Misiewicz, B. Paszkiewicz, R. Paszkiewicz, M. Tłaczała, Contactless electroreflectance study of band bending for undoped, Si- and Mg-doped GaN layers and AlGaN/GaN transistor heterostructures, Microelectronics Journal **40**, 370 (2009).

[24] http://www.nextnano.de/

[25] A. Gocalinska, S. Rubini, E. Pelucchi, Native oxides formation and surface wettability of epitaxial III–V materials: The case of InP and GaAs, Appl. Surf. Sci. **383**, 19 (2016).

Accepted Manuscript

Figure captions:

FIG. 1. (a) Diagram of layer sequence in examined InAlAs van Hoof structures. Sketch of band bending in *n*-type (b) and *p*-type (c) InAlAs van Hoof structures in the presence of surface Fermi level pinning.

FIG. 2. Contactless electroreflectance spectra of *n*-type InAlAs van Hoof structures of various thicknesses *d* of undoped top InAlAs layer. The grey lines correspond to measurements performed about one year later at similar conditions. FKO extrema are identified and signed with numbers. Inset shows piezorflectance spectrum for the structures with 120 nm thick undoped InAlAs layer.

FIG. 3. Contactless electroreflectance spectra of *p*-type InAlAs van Hoof structures of various thicknesses *d* of undoped top InAlAs layer. The grey lines correspond to measurements performed about one year later at similar conditions. FKO extrema are identified and signed with numbers.

FIG. 4. Analysis of built-in electric field in *n*-type (a) and *p*-type (b) InAlAs van Hoof structures. Solid lines are best fit to experimental points and calculated slopes determines electric field *F* for the undoped InAlAs layer of various thicknesses.

FIG. 5. Built-in electric field in *n*-type (red squares) and *p*-type (blue diamonds) InAlAs van Hoof structures, fitted by formula $F = \frac{E_\phi}{d}$ for *n*-type and $F = \frac{E_g - E_\phi}{d}$ for *p*-type structures, where *d* is the thickness of undoped InAlAs layer, *F* is the built-in electric field extracted from FKO analysis, and the E_ϕ is treated as a free parameter.

Accepted Manuscript

FIG. 6. Theoretical dependence of built-in electric field on potential barrier height (solid lines) for *n*-type (a) and *p*-type (b) InAlAs van Hoof structures of various thicknesses *d* of undoped InAlAs layer. Thick horizontal solid lines correspond to experimental values of *F*.

FIG. 7. Band diagram showing the calculated band bending in *n*-type (left panel) and *p*-type (right panel) InAlAs van Hoof structures of various thicknesses *d* of undoped InAlAs layer. Gray fields indicate the depletion regions in the doped InAlAs layer. Grey dashed lines indicate the Fermi level in structures. E_ϕ is assumed to be located 0.73eV below the conduction band for all InAlAs van Hoof structures.

FIG. 8. The atomic concentration of a surface atoms identified on InAlAs van Hoof structures by XPS measurements. Inset shows an exemplary XPS spectrum from the n-type van Hoof structure.

FIG. 9. AFM surface morphology (signal amplitude) of a representative InAlAs sample grown on InP (100) + 0.4° tow. [111]A substrate, stored in ambient conditions for several months after growth. (AFM collected in non-contact/tapping mode, at room temperature and in air)

Accepted Manuscript

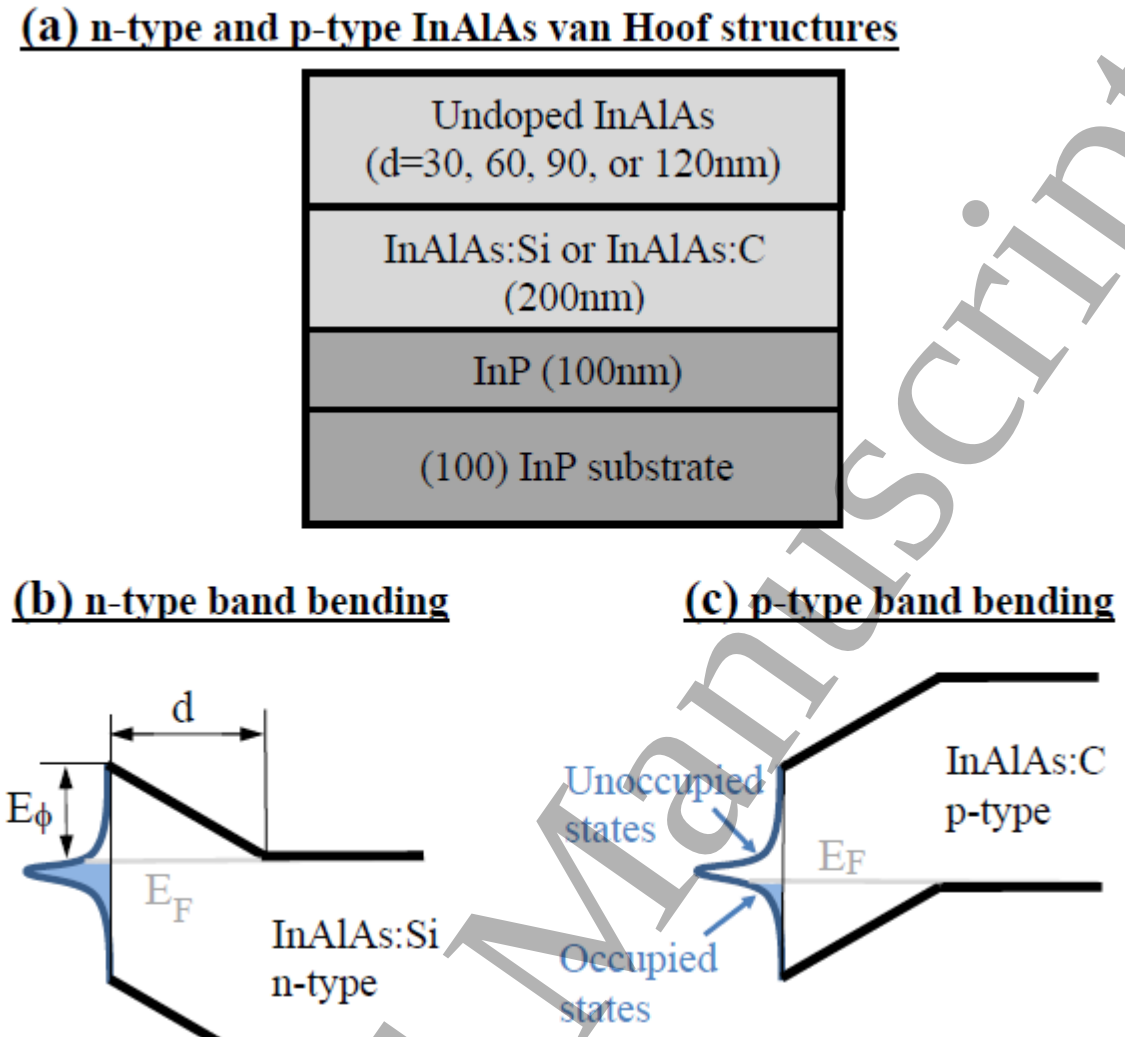


FIG. 1.

(A. Tolloczko et al.)

Accepted Manuscript

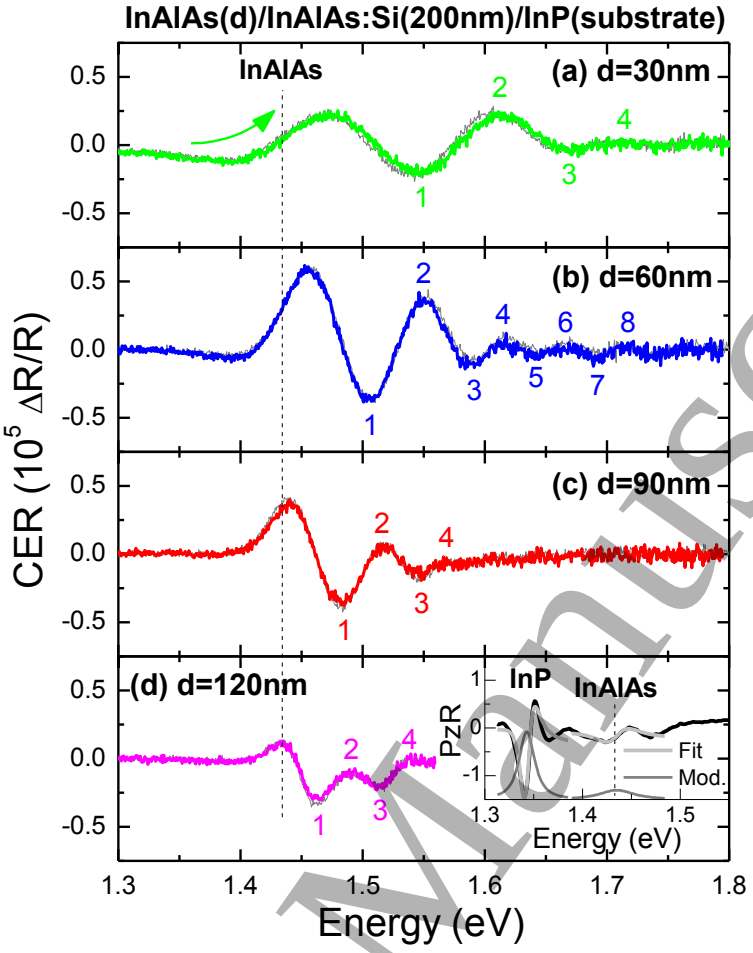


FIG. 2.

(A. Tolloczko et al.)

Accepted Manuscript

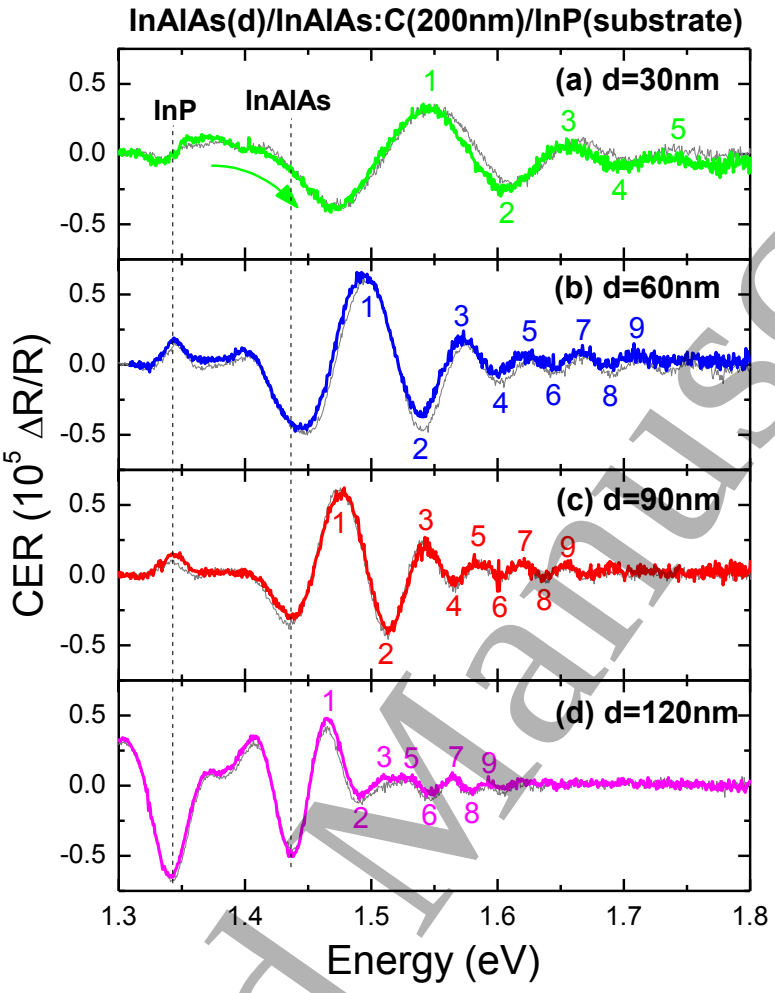


FIG. 3.

(A. Tolloczko et al.)

Accepted Manuscript

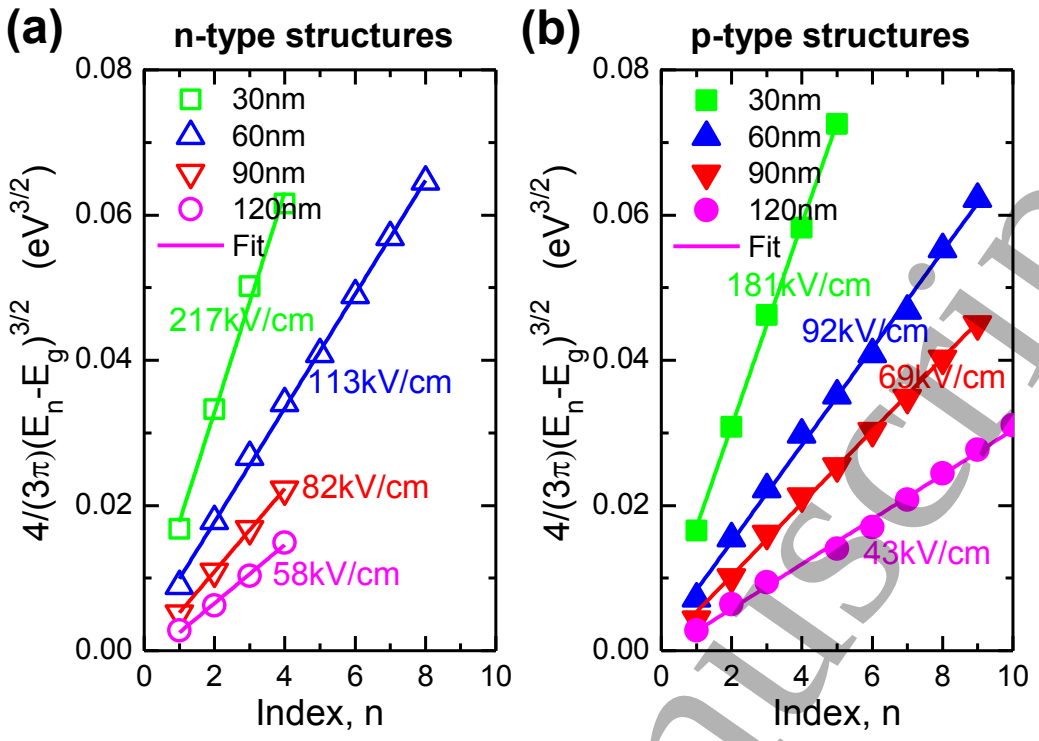


FIG. 4.

(A. Tolloczko et al.)

Accepted Manuscript

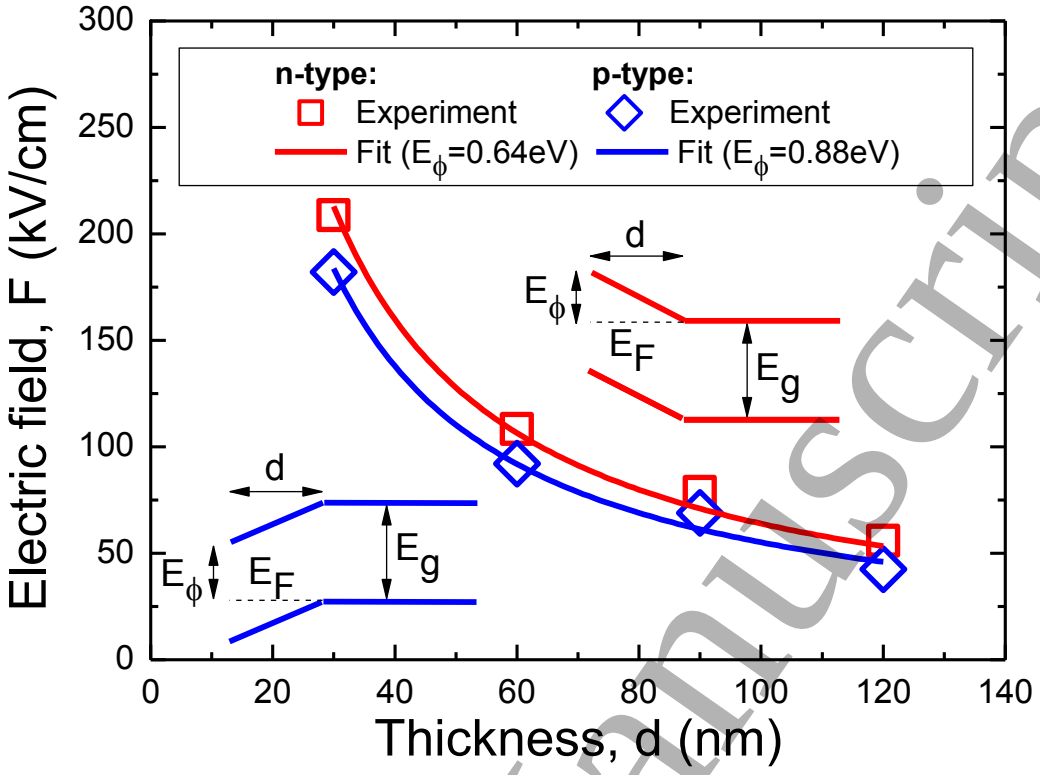


FIG. 5.

(A. Tolloczko et al.)

Accepted Manuscript

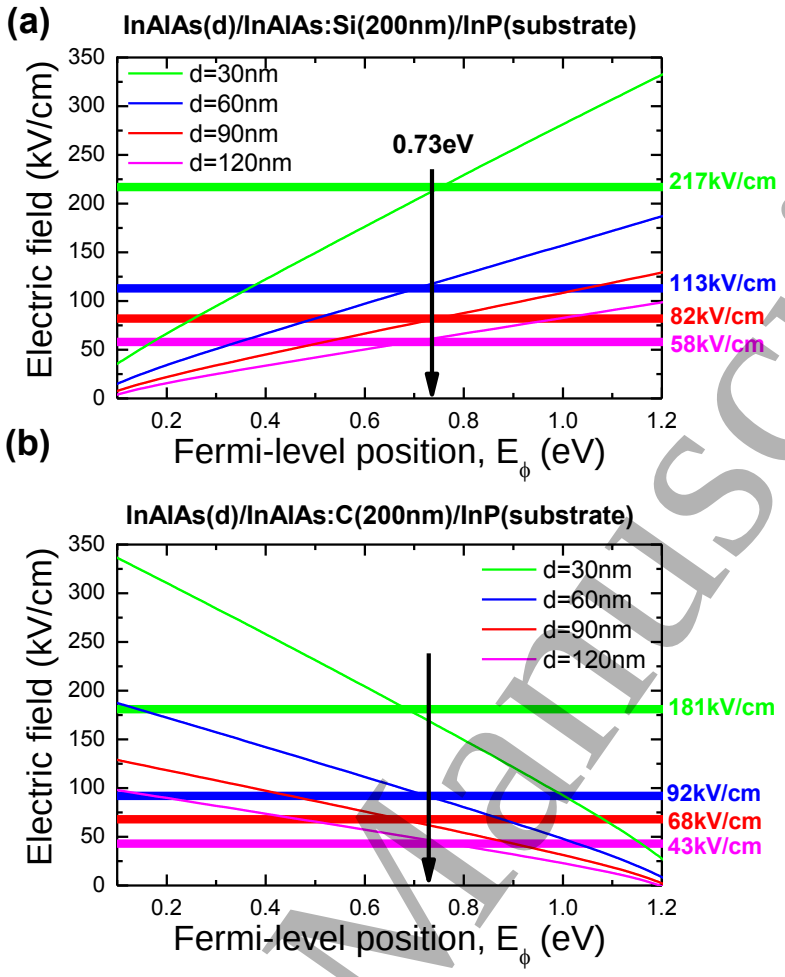


FIG. 6.

(A. Tolloczko et al.)

Accepted Manuscript

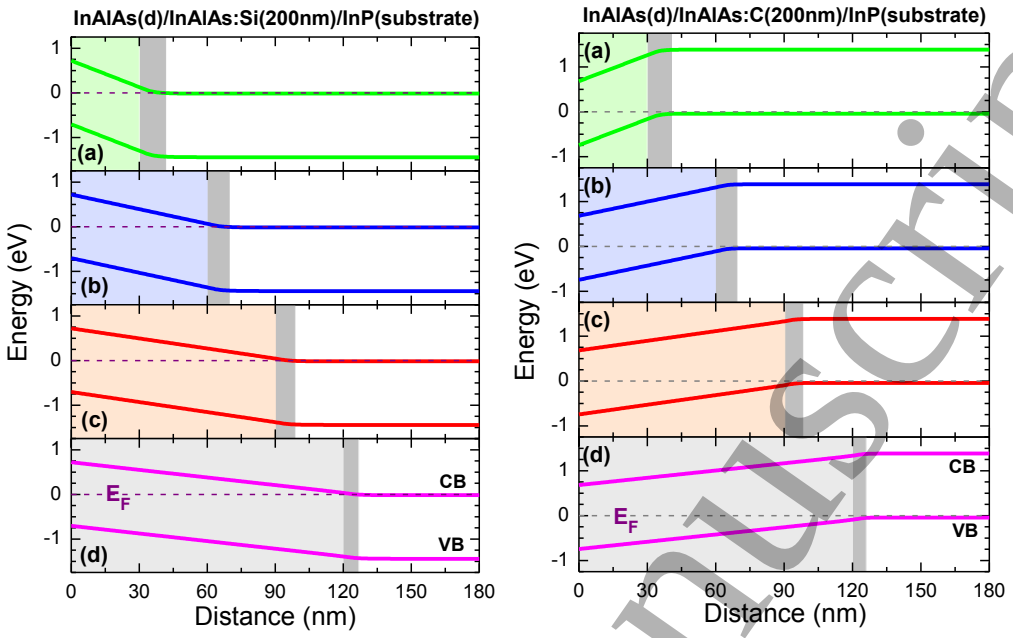


FIG. 7.

(A. Tolloczko et al.)

Accepted Manuscript

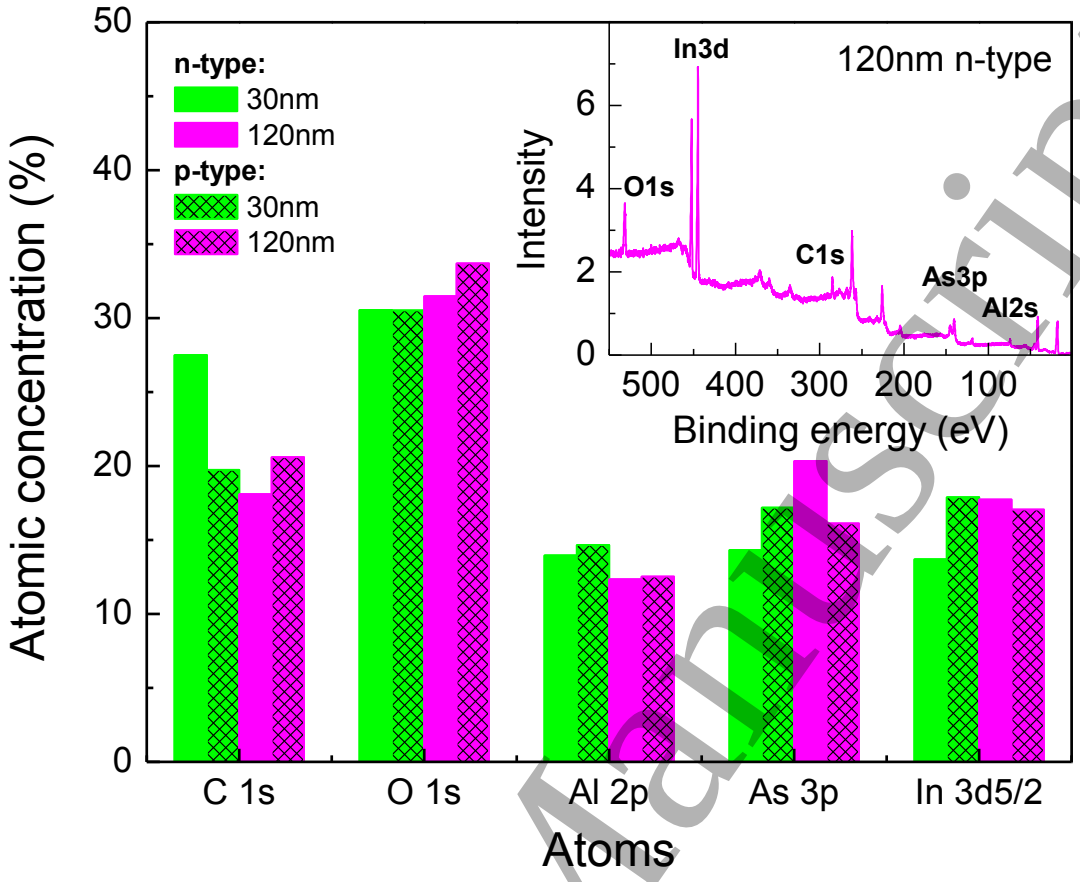


FIG. 8.

(A. Tolloczko et al.)

Accepted Manuscript

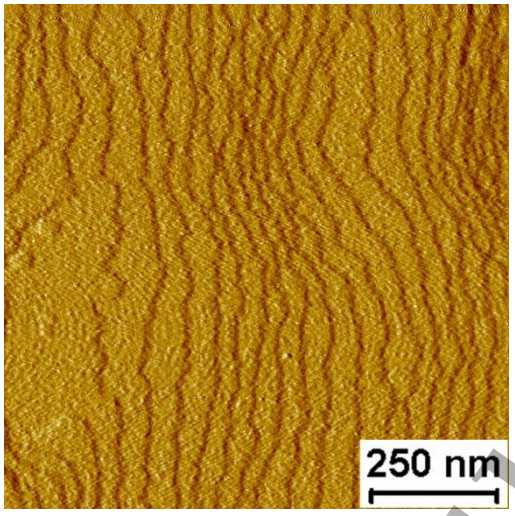


FIG. 9.

(A. Tolloczko et al.)

Accepted Manuscript